

# Ancient Great Wall Building Materials Reveal Paleoenvironmental Changes in Northwestern China

Robert Patalano (✉ [patalano@shh.mpg.de](mailto:patalano@shh.mpg.de))

Max Planck Institute for the Science of Human History <https://orcid.org/0000-0002-9075-4556>

Jing Hu

Chinese Academy of Sciences

Qing Leng

Bryant University

Weiguo Liu

Chinese Academy of Sciences

Huanye Wang

Chinese Academy of Sciences

Patrick Roberts

Max Planck Institute for the Science of Human History

Michael Storozum

The Hebrew University of Jerusalem

Lin Yang

National Museum of China

Hong Yang

Bryant University

---

## Article

**Keywords:** Great Wall, plant material, construction

**DOI:** <https://doi.org/10.21203/rs.3.rs-390056/v1>

**License:**   This work is licensed under a Creative Commons Attribution 4.0 International License.

[Read Full License](#)

---

# Abstract

Plant material used in the construction of segments and beacon towers of the ancient Great Wall in northwestern China contain untapped potential for revealing paleoenvironmental conditions. Here, we characterize the molecular preservation and stable carbon and nitrogen isotope compositions of common reeds (*Phragmites*) collected from Great Wall fascines dated to the Han Dynasty in today's Gansu and Xinjiang provinces using a combination of chromatographic techniques and isotope analyses. Our data demonstrates that ancient reeds were harvested from local habitats that were more diverse than exist today. The isotope data also capture differential rates of environmental deterioration along the eastern margin of the Tarim Basin, leading to the intense evaporative stress on modern plants. This study demonstrates the wealth of environmental and climate information obtainable from site-specific organic building material of ancient walls, which have received considerably less attention than the iconic brick and stone masonry walls of the later Ming Dynasty.

## Introduction

As one of the most recognizable world heritage sites, the Great Wall of China is a manifestation of the engineering capabilities and architectural achievements of multiple Chinese dynasties<sup>1</sup>. What is perhaps less well known, is that the iconic brick walls built during the Ming Dynasty in the 15th Century AD<sup>2</sup>, which extend between Jiayuguan in Gansu Province and Shanhaiguan in Hebei Province, are only part of a series of multi-material fortifications that stretch across northern China<sup>1,3-7</sup>. Indeed, as early as the 2nd century BC, an extensive system of fascine and rammed-earth walls, beacon towers, and fortifications expanded the western frontier of the Han Empire from the central plains into today's Gansu Province and Xinjiang Uyghur Autonomous Region (Figs. 1 and 2; Supplementary Table 1).

Constructed using locally available materials such as reed fascines and wood bundles interbedded with gravel-mixed rammed earth, the early Great Wall was constructed along the northern edge of the Tibetan Plateau extending to the eastern Tarim Basin. The building projects lasted for a few hundred years and through a series of dynastic changes and global and regional climatic fluctuations<sup>4,8</sup>. Although over the past two millennia much of the Han era walls and beacon towers have become fragmented ruins, some sections in Gansu and Xinjiang are well preserved due to the arid continental climate<sup>9</sup>. While remnants of the Han Dynasty walls along the Shule River in Gansu and Inner Mongolia Autonomous Region have been surveyed and studied<sup>10-13</sup>, isolated beacon towers (Fig. 2C) along the Kongque River (Fig. 1B) in the arid areas of Xinjiang are relatively unknown despite being described in ancient historical documentation such as the 5th Century AD "Book of Later Han"<sup>14</sup>. Built along the ancient Silk Road, these towers and fortifications served as a military communication and warning system, symbolic political borders, and rest stops for traveling merchants<sup>4,6,7,15</sup>.

Today, a large portion of northwestern China, including Xinjiang, the Hexi Corridor in Gansu, and the area west of the Helan Mountains of Inner Mongolia, has a semi-arid to arid continental climate with hot

summers and cool, dry winters characterized by low rainfall and prolonged droughts<sup>16,17</sup> (Supplementary Fig. 1). Desertification brought on by natural climate changes<sup>18,19</sup> amplified by human activity<sup>20</sup>, has resulted in severe evapotranspiration<sup>21</sup> and the proliferation of desert and xeric shrubland plant species in the region<sup>22</sup>. Such changes have potential historical corollaries, however, as intensive irrigated farming and an overdraw of highland tributaries during the Han Dynasty is believed to have changed local hydroclimate, reduced water levels, and led to the salinification of lakes bordering the Tarim Basin, such as Lop Nur<sup>23,24</sup>.

Although extensive lacustrine<sup>25–33</sup>, speleothem<sup>34,35</sup>, and ice core<sup>36,37</sup> records exist from northwestern China for the Han period, many of these are off-site archives that do not necessarily show changes at local scales. The eastern Tarim Basin is a key geographical crossroads between Central and East Asia, holding political, military, cultural and economic significance historically<sup>6</sup>, and was subject to both imperial expansion and agricultural intensification in the Late Holocene<sup>9,24,33,38,39</sup>. The walls, small and large forts, beacon towers, lookout platforms, watchtowers, and other structures were constantly refortified with locally available plants<sup>5</sup>. As a result, the biomolecular contents of these organic materials within preserved ramparts may contain evidence of environmental conditions at specific historical points along the Great Wall in China's arid northwest.

*Phragmites* Adanson (Poaceae family), the cosmopolitan common reed, is the most common plant found in these ancient structures as a natural building material. This reed was used in Neolithic shelters<sup>3</sup>, and continues to be harvested for use in construction in oases of dry central Asia today. *Phragmites* is a highly successful C<sub>3</sub> plant genus, has considerable variation with high phenotypic plasticity, a wide geographic distribution, and the ability to occupy aquatic and marginal habitats under various climate conditions<sup>40,41</sup>. Despite geochemical analyses on tissues from living *Phragmites*<sup>42–44</sup>, reports on its pollen<sup>45</sup> and phytolith records<sup>46</sup> in archaeological contexts, and the identification of a rope made from culms (stems) of *Phragmites* at Gumugou Cemetery, a site dated to 3800 years cal BP and ~ 70 km east of Lop Nur<sup>47</sup>, no molecular characterization or isotope measurements have been taken on the ancient remains of *Phragmites* collected from the Great Wall itself.

Here, we investigate plant material preserved in fascines of the Great Wall sections and beacon towers dated to the Han Dynasty from Gansu and Xinjiang to reveal the ecological and environmental dynamics of early Chinese historical periods at the onset of intensified human landscape modification.

## Results

### Py-GC-MS Analysis

The lignin and polysaccharide pyrolysates, which dominate the molecular composition of ancient culms from Great Wall segments, beacon towers and fortifications, have a similar distribution of compounds when compared to modern *P. australis* (Fig. 3 & Supplementary Table 2). However, the ancient samples

contain some compounds that are not in modern analogs, such as apocynin and desaspidinol. Pyrolysis products in extant culm and leaf samples are similar and include benzene and furan derivatives, phenol derivatives, and indole derivatives of amino acids. Lignin moieties contain phenol, methyl and methoxy phenol, vinyl phenol, and vanillin, while polysaccharide moieties include furans and furfural, benzofuran, and levoglucosan. Lipids are detected in modern samples as primarily palmitic (C<sub>16</sub>) and stearic (C<sub>18</sub>) acids, but dodecanoic (C<sub>12</sub>) and tetradecanoic (C<sub>13</sub>) acids were identified in only one sample, a *P. australis* leaf collected along the roadside near Yumenguan (Site 5). Indoles (e.g., Indole, 3-methyl-) indicate the presence of amino acids, but sitosterol is present in the *P. australis* leaf sample from Milan Castle fortification (Site 8). Overall, for each site, pyrolysis data indicate that modern culms and leaves preserve a similar suite of compounds, apart from the leaves containing more abundant fatty acids (Fig. 3 and Supplementary Table 2). Variation exists in compound distribution among ancient samples collected from different sites. Ancient samples from Yumenguan (Site 5) have fewer lignin derivatives but contain identifiable fatty acids, whereas the Majuanwan (Site 7) samples have more abundant lignin derivatives but fewer overall polysaccharide compounds (Supplementary Fig. 2).

### Lipid Concentration and Distribution

The concentration of *n*-alkanes (C<sub>21</sub>-C<sub>33</sub>) is approximately 10-times lower in ancient samples than in their modern analogs. On average, modern culms contain 13,641 µg of C<sub>21</sub>-C<sub>33</sub> *n*-alkanes per gram of dry material (µg/g) (Std. Dev. = 7,849; *n* = 13), whereas ancient culms yield on average 1,325 µg/g (Std. Dev. = 1,771; *n* = 33). Overall, there is a significant difference in C<sub>21</sub>-C<sub>33</sub> *n*-alkane abundance between modern and ancient samples as shown by a Student's t-test (two-tailed, *p* = 0.0001).

Figure 4 shows the ternary diagrams of the C<sub>27</sub>, C<sub>29</sub>, and C<sub>31</sub> relative abundances for *n*-alkanes from ancient and modern *Phragmites*. Of the 33 ancient samples containing enough lipid material for GC-MS analysis, 13 (39.4%) have C<sub>27</sub> as the most dominant *n*-alkane, while C<sub>29</sub> and C<sub>31</sub> *n*-alkanes are most abundant in nine (27.2%) and eight (24.2%) samples, respectively. Two samples (6.1%) from Yingpan City Heritage Site (Sites 9, 10) have C<sub>23</sub> as the leading *n*-alkane, while one sample from Sishilidadun Tower (Site 14) has C<sub>21</sub> as the most abundant (3.0%). In samples with C<sub>27</sub> as the most abundant compound, all but three have C<sub>29</sub> as the second most dominant *n*-alkane; two have C<sub>25</sub>, and one sample has C<sub>31</sub> as the second most abundant compound (Fig. 5). This wide distribution of lipid profiles contrasts with modern reeds, in which 9 of the 12 samples (75%) have the C<sub>29</sub> homologue as the most dominant compound, while two samples (16%) have C<sub>27</sub> as the most abundant alkane, and one sample (8%) has C<sub>31</sub> (Supplementary Fig. 3).

The average chain length (ACL<sub>21-33</sub>) ranges from 22.8 to 30 (Avg. 27.9; *n* = 33) for ancient samples, overlapping with the distribution of ACL in modern reeds of 26.4 to 31 (Avg. 28.1; *n* = 12) (Fig. 6). This is consistent with previous reports of modern *Phragmites* ACL from China<sup>42-44,48</sup>. There are no significant differences in ACL values between modern and ancient reeds in a Student's t-test for ACL<sub>21-33</sub> values (two-tailed, *p* = 0.7588). The CPI of the C<sub>21</sub>-C<sub>33</sub> *n*-alkanes ranges between 2.0 and 19.3 (Avg. 7.3; *n* = 33)

and 3.8 and 23.2 (Avg. 8.2;  $n = 12$ ) in ancient and modern reeds, respectively. These values are typical of plant-derived CPI values<sup>49</sup>, and indicate that no significant degradation occurred in the longer chain compounds of the ancient reeds.

## Bulk Carbon and Nitrogen Isotope Analysis

Ancient reeds yield bulk  $\delta^{13}\text{C}$  between  $-25.3\text{‰}$  and  $-22.6\text{‰}$  (Avg.  $-23.9\text{‰}$ ;  $n = 42$ ), whereas modern bulk  $\delta^{13}\text{C}$  corrected for the Suess effect range between  $-24.6\text{‰}$  and  $-20.8\text{‰}$  (Avg.  $-22.9\text{‰}$ ;  $n = 12$ ) (Fig. 7; Supplementary Table 1). There is a significant difference between corrected modern and ancient reeds in a Student's t-test (two-tailed,  $p = 0.0178$ ).

Modern *P. australis* also exhibit significant differences in  $\delta^{13}\text{C}$  between samples from eastern ( $n = 7$ ) and western ( $n = 5$ ) clusters (Student's t-test two-tailed,  $p = 0.0009$ ). Western cluster samples are  $+2.0\text{‰}$  heavier than eastern samples with average corrected  $\delta^{13}\text{C}$  of  $-21.7\text{‰}$  and  $-23.7\text{‰}$ , respectively. In ancient samples, however, eastern sample  $\delta^{13}\text{C}$  averages  $-23.7\text{‰}$  ( $n = 26$ ), only  $+0.5\text{‰}$  heavier than those from the western cluster ( $-24.2\text{‰}$ ;  $n = 16$ ).

There is no significant difference between corrected modern ( $n = 7$ ) and ancient ( $n = 26$ )  $\delta^{13}\text{C}$  in the eastern cluster (Student's t-test two-tailed,  $p = 0.9$ ), and both have an average  $\delta^{13}\text{C}$  of  $-23.7\text{‰}$ . On the other hand, there is a significant difference between corrected modern ( $n = 5$ ) and ancient ( $n = 16$ )  $\delta^{13}\text{C}$  in the western cluster (Student's t-test two-tailed,  $p = 0.0002$ ), as corrected modern samples have an average  $\delta^{13}\text{C}$  of  $-21.7\text{‰}$  compared to the ancient sample average  $\delta^{13}\text{C}$  of  $-24.2\text{‰}$  (Fig. 7).

Ancient reed bulk samples yield large variations in  $\delta^{15}\text{N}$  with values ranging from  $+0.8\text{‰}$  to  $+33.5\text{‰}$  (Avg.  $+9.3\text{‰}$ ;  $n = 42$ ). Reed  $\delta^{15}\text{N}$  signals have a strong tendency to be site specific, with samples from the Milan Castle Heritage Site (Site 8) (Avg.  $\delta^{15}\text{N}$   $27.5\text{‰}$ ;  $n = 3$ ) and the Sishilidun Beacon Tower (Site 14) (Avg.  $\delta^{15}\text{N}$   $15.9\text{‰}$ ;  $n = 3$ ) being significantly higher compared to all other sites (Avg.  $\delta^{15}\text{N}$   $+7.2\text{‰}$ ;  $n = 36$ ) (Fig. 8). In general,  $\delta^{15}\text{N}$  in ancient eastern cluster (Avg.  $\delta^{15}\text{N}$   $+6.9\text{‰}$ ;  $n = 26$ ) samples tend to be lower than that from the western cluster (Avg.  $\delta^{15}\text{N}$   $+13.0\text{‰}$ ;  $n = 16$ ) sites (Student's t-test two-tailed,  $p = 0.0171$ ), adhering to global patterns of the  $\delta^{15}\text{N}$  composition of plant and soil nitrogen across temperature and precipitation gradients<sup>50</sup>. At the Sishilidun Beacon Tower (Site 14), the only location where  $\delta^{15}\text{N}$  was measured on both modern and ancient reeds, extant plants yield an average  $\delta^{15}\text{N}$  of  $+0.7\text{‰}$  ( $n = 3$ ), a sharp contrast to  $+15.9\text{‰}$  in ancient samples.

## Discussion

### Differential Rates of Environmental Deterioration

Located at the center of the Eurasian continent, the Tarim Basin is now an extremely arid region containing the Taklamakan Desert, the world's second largest shifting sand desert. Annual precipitation is between 50–80 mm on the basin's edges and only 17–25 mm at the center, with evaporation that can

reach as high as 1500 mm yearly<sup>51,52</sup>. Temperature records in Xinjiang indicate that the Tarim Basin experienced significant, monotonic warming with an average increase of nearly 1°C from 1955 to 2000, unevenly distributed across time and space<sup>51</sup>. While relatively wet climate conditions are inferred for western China during the Han Dynasty<sup>25–37</sup>, environmental deterioration is evident around the eastern Tarim Basin<sup>23</sup>. The dramatic transformation in hydroclimate is apparent at Lop Nur which experienced its lowest lake levels or first periods of desiccation at the end of the Han Dynasty (220 BC)<sup>31</sup>. Overuse of water resources resulted in settlement abandonment in this sensitive ecoregion, ultimately leading to desertification in northwestern China over the last two millennia<sup>24,36,53</sup>. Our bulk carbon isotope data capture the differential rates of change on both sides of Lop Nur, when comparing ancient and modern material.

Although we are unable to infer the degree to which Han agricultural intensification led to landscape degradation in and around wall segments or beacon towers because our time window is rather limited, we can confirm different rates of changes in ancient climate parameters (i.e., temperature and precipitation) between the eastern and western clusters of the Lop Nur basin. The average  $\delta^{13}\text{C}$  from ancient reeds is relatively uniform across all sampling locations (-23.9‰;  $n = 42$ ), with western sites (-24.2‰;  $n = 16$ ) being on average only - 0.5‰ lighter than their eastern counterparts (-23.7‰;  $n = 26$ ). This uniformity was likely due to the relatively wetter and homogeneous conditions in the eastern Tarim Basin for the Han Dynasty, coinciding with the stronger Asian monsoon<sup>18,19</sup>. It is also consistent with other proxies from the region showing a wetter climate<sup>31,36</sup>. However, average  $\delta^{15}\text{N}$  is different across clusters, with western sites (+ 13.0‰;  $n = 16$ ) being on average + 6.1‰ heavier than their eastern counterparts (+ 6.9‰;  $n = 26$ ), including some extremely heavy values at the Milan Castle fortification (Site 8) and the Sishilidadun Beacon Tower (Site 14). As  $\delta^{15}\text{N}$  values of plant roots, plant litter, and soil organic matter decrease with increasing precipitation<sup>50,54</sup>, it is possible that the east of Lop Nur was already wetter and cooler than to the west of the lake during the Han Dynasty.

There is a + 2.0‰ difference in carbon isotope values between modern *Phragmites* growing in eastern (-23.7‰) and western (-21.7‰) clusters, a striking contrast from the small  $\delta^{13}\text{C}$  offset pattern observed in ancient samples (Fig. 8). Additionally, the + 2.5‰ heavier  $\delta^{13}\text{C}$  values in the modern western samples compared to the ancient analogs suggests a differential rate of environmental change across the eastern edge of the Tarim Basin, specifically on opposite sides of Lop Nur.

The  $^{13}\text{C}$  enrichment in the modern western cluster can be attributed to increased water-use efficiency resulting from higher rates of evapotranspiration under extremely arid conditions<sup>55,56</sup>. Carbon isotope ratios can be used as indicators of plant water-use efficiency (WUE)<sup>55,56</sup>, and plants in arid environments that are more efficient are proportionally enriched in  $^{13}\text{C}$  compared to well-watered varieties<sup>55</sup>. Annual temperature and precipitation at Yuli, which represents our western cluster samples' climate parameters, averages 12.1°C and 37.2 mm, respectively. This is ~ 5°C warmer and half the annual precipitation of that in Yumen from east of Lop Nur (Supplementary Fig. 1). Thus, the extensive aridity and higher

evapotranspiration under which modern *Phragmites* grow in the western cluster has a significant fractionation effect on bulk carbon isotope values, resulting in heavier  $\delta^{13}\text{C}$ . The + 2.5‰ average  $\delta^{13}\text{C}$  values in modern western reeds shows that 21st Century warming has had a larger effect on bulk  $\delta^{13}\text{C}$ , driving values higher than otherwise expected regardless of atmospheric  $\text{CO}_2$   $^{13}\text{C}$  depletion. For example, at the two sites at the Yingpan City (Sites 9 and 10), corrected modern samples are + 3.0‰ and + 2.2‰ higher on average than ancient reeds, respectively. Additionally, modern samples are + 2.9‰ higher on average than ancient reeds at the Sishilidun Beacon Tower (Site 14). While both regions have become warmer and dryer since the Han Dynasty<sup>24,36,53</sup>,  $\delta^{13}\text{C}$  data from these sites suggest that there is a faster rate of change in the western cluster near the Taklamakan Desert due to elevated temperatures and a higher degree of aridity and evapotranspiration. Whether this is due to natural forcing<sup>19,36</sup> or human-induced changes in hydroclimate<sup>31,53</sup>, is currently unresolved.

### Temperature and the Diversity of Ancient *Phragmites* Populations

The wider distribution and higher variation of *n*-alkanes in ancient reeds from different sites contrasts with that of modern samples, suggesting that ancient *Phragmites* occupied more diverse and heterogeneous habitats. Research into *n*-alkane chain length distributions in *P. australis* in the central Chinese Loess Plateau<sup>43</sup> and from Yellow River estuarine wetlands<sup>42</sup> found that  $\text{C}_{31}$  is the most dominant compound in the extant population. On the other hand, the  $\text{C}_{29}$  *n*-alkane dominates *P. australis* lipids in lakeside habitats in England<sup>57</sup>. However, a study<sup>44</sup> on the distribution and isotopic composition of *n*-alkanes from *P. australis* growing along a latitudinal gradient across China shows a correlation between dominant compound and ACL with temperature; that is, higher ACL and carbon chains coincide with higher temperatures. The relative abundance of specific *n*-alkanes correlates with temperature in other plant species, too<sup>58–63</sup>. The high variations of *n*-alkane distribution and more diverse chain dominance (Fig. 6) in each ancient site reflect the existence of ecological variations in the past, further supporting the existence of wetter, more diverse habitats in the past.

The  $\text{C}_{29}$  *n*-alkane is most abundant in 75% (9 of 12) of our modern *P. australis* samples, whereas  $\text{C}_{29}$  is dominant in only 27.2% (9 of 33) of the ancient reeds.  $\text{C}_{27}$  is the most dominant *n*-alkane in the ancient samples, but only by a narrow margin (39.4%) as both  $\text{C}_{29}$  and  $\text{C}_{31}$  (24.2%) are found in good quantity. As there is no clear distinction in dominant chain length distribution in ancient samples by site, apart from the Han Great Wall Heritage Site (Site 6) and the Sunji Beacon Tower (Site 12), we suggest that there were likely more heterogeneous habitats present when the walls and beacon towers were built. Furthermore, both the mixed chain length distribution observed in the ancient *Phragmites* samples and the  $\delta^{13}\text{C}$  data advocate for more uniform climate parameters east and west of the Lop Nur basin and a greater wetland extent in the past. For example, proximity to water may have resulted in *Phragmites* with lower *n*-alkane chains dominating lipid profiles, such as at the Yingpan City Heritage Site (Sites 9, 10) and Sishilidun Tower (Site 14).

In many aspects, the Sishilidadun Tower (Site 14) stands out among other sites for its lipid distribution, abundance of the C<sub>21</sub> homologue, and significantly lower ACL<sub>21-33</sub> value. The lower ACL (24.3) and relative abundance of the C<sub>21</sub> *n*-alkane likely implies that these reeds were harvested from a wetland or swamp habitat when the tower was fortified. Low- to mid-chain homologues (C<sub>21</sub>-C<sub>25</sub> *n*-alkanes) dominate plants occupying wetter habitats such as submerged and floating aquatic macrophytes<sup>57,64,65</sup>. Conversely, long-chains (C<sub>27</sub>-C<sub>35</sub> *n*-alkanes) are more abundant in terrestrial plants<sup>66,67</sup>. Although the mechanism for the affinity between higher mid-chain *n*-alkane homologues and wetland conditions is not well understood<sup>63,68-70</sup>, the relative abundance of C<sub>21</sub>-C<sub>25</sub> alkanes in the Sishilidadun Tower samples may suggest more humid conditions affiliated with the site's proximity to Bosten Lake. This is supported by the carbon isotope data, as two Sishilidadun samples have the lowest δ<sup>13</sup>C values recorded, ~-25‰, and C<sub>3</sub> plants in wetter environments are proportionally depleted in <sup>13</sup>C compared to arid-adapted analogs<sup>55</sup>.

Our measured ACL values from both ancient and modern *Phragmites* are within the range of previously reported values from modern samples of the genus<sup>42,44</sup>. Although there was no significant difference in ACL<sub>21-33</sub> values between all modern and ancient reeds in a Student's t-test (two-tailed, *p* = 0.07588), ACL<sub>21-33</sub> tracks higher in all modern samples from individual sites where both were sampled, except Majuanwan (Fig. 7). ACL values correlate with higher growing season temperature and aridity<sup>58,59,61</sup> and therefore, the higher ACL values in modern plants are consistent with elevated temperatures in northwestern China following intensive irrigation farming that began in the middle of the 20th Century<sup>23</sup>, or the nearly 1°C yearly increase in the region over the past 50 years<sup>51</sup>. Selective pressures may favor the production of longer *n*-alkane chain lengths under hot or arid conditions<sup>63,71</sup>, and extant *P. australis* likely suffer from water stress brought on by significant evapotranspiration, which drives ACL values higher.

## Archaeological Significance of the Great Wall in Northwestern China

Although the rammed-earth Han Dynasty segments of the Great Wall do not elicit the amount of attention as the brick and stone masonry of the Ming Dynasty portions of the Great Wall, they offer a wealth of information on the sourcing of natural organic building materials and paleoclimatic and environmental signals they contain. As the morphology predicted, ancient reeds from walls and towers show good molecular preservation with abundant polysaccharide and lignin, as detected by Py-GC-MS (Fig. 3). Ancient reed culms have a similar suite of pyrolysis products as their modern homologues, apart from identifiable amino acids and relatively lower amounts of fatty acids which are attributed to decay over the past two millennia. Ancient samples also contain compounds that are not identified in modern *Phragmites*, such as apocynin and desaspidinol, interpreted as lignin decomposition products<sup>72</sup> or possible indicators of hardwood<sup>73</sup>. As hardwood species such as *Tamarix sp.* was sometimes mixed with *Phragmites* in Great Wall fascines<sup>1</sup>, it is therefore possible that the presence of these compounds are due to cross-contamination from the building process. Consistent with the Py-GC-MS data, the CPI of the C<sub>21</sub>-C<sub>33</sub> *n*-alkanes (Fig. 7) implies that degradation for long chain *n*-alkanes is minimal, likely due to the dry

regional climate helping to preserve organic archaeological remains<sup>9</sup>. Although the wide CPI range observed in living plants (between 2.1 and 16.7) precludes its use as a single metric on which to base sample integrity<sup>49</sup>, land plants typically display CPI values  $> 5.0$ , while mature or heavily degraded samples are characterized by a considerably lower CPI of  $\leq 1.0$ . Overall, with minor variation of Py-GC-MS moieties among different sites, ancient culms exhibit excellent molecular preservation with abundant labile biomolecules. Although containing a lower quantity of lipids, ancient culms from these ancient wall segments or beacon towers yielded diverse *n*-alkanes that are comparable with their distributions in modern leaves.

The variation in pyrolysis products between culms and leaves, as well as among samples across sites, is also expected given the difference in the chemical composition between the two plant parts. The excellent preservation of these organic building materials suggests that the absence of *Phragmites* leaves and inflorescences/infructescences in the walls was intentional, and culms were selected as building material due to its high lignin fiber content that provided strength and durability. Moreover, distinct lipid profiles and isotope data from samples at individual wall segments and beacon towers support historical evidence that construction material was sourced from locally available plants<sup>1,5</sup>. The reeds used for the construction of Milan Castle fortification (Site 8) for instance, yield heavy average  $\delta^{15}\text{N}$  value of  $+ 27.5\text{‰}$ , while the Cang Ting Sui Beacon Tower (Site 5) and wall segments at the Great Wall Heritage Site (Site 6), locations which are only 5 km apart, have average  $\delta^{15}\text{N}$  values of  $+ 8.3\text{‰}$  and  $+ 2.0\text{‰}$ , respectively. The regional differences likely reflect differences in the use of fertilizers around larger population centers like the Milan Castle, which may have resulted in the extremely heavy  $\delta^{15}\text{N}$  values (Fig. 8)<sup>74-76</sup> as fertilizers derived from manures or guano are enriched in  $^{15}\text{N}$  and would have an impact on local plant isotopic values<sup>50,77</sup>. Nonetheless, the unusually high nitrogen isotope compositions detected in ancient reeds deserve further investigation.

The regional environmental change in China's northwestern frontier is an explicit concern in the discussion of various episodes of migrations and cross-cultural exchanges of technologies, military, farming, and pastoral activities as the eastern Tarim Basin has been a crossroad location in those narratives. The causes of the environmental alteration and deteriorations have been debated as to whether it results from natural forcing such as the change of Asian monsoon strength<sup>18,19</sup> or from intensified agricultural activities<sup>23,31</sup>. Despite farming activities documented in prehistoric archaeology in the region, agricultural intensification in northwestern China can be traced back to when the Han Dynasty implemented the *Tuntian* system of organized military farming<sup>20</sup>. This was first employed in the Hexi Corridor and later extended into the empire's western regions, allowing for territorial expansion across the ancient Silk Road from Dunhuang to Central Asia and through the Tarim Basin between the Kunlun and Tianshan Mountains<sup>20</sup>. However, we cannot currently state with confidence the degree to which past human land-use changes influenced the hydroclimate and environments of northwestern China until additional samples are collected and analyzed. Nevertheless, this work highlights the excellent preservation of the organic materials in ancient Great Wall segments and beacon towers and their potential for paleoenvironmental reconstructions. Along with other regional and global climate proxies,

they illuminate site-specific environmental records that speak to localized natural or human-induced environmental change in northwestern China. More research based upon higher resolution sampling strategies with other molecular isotope climate proxies from additional newly surveyed beacon towers in Xinjiang will certainly yield valuable information; given the abundance and excellent molecular preservation of these ancient *Phragmites*, such studies are warranted.

## Conclusions

Ancient reeds, *Phragmites*, used in Han Dynasty Great Wall segments, beacon towers, and fortifications demonstrate excellent molecular preservation showing the potential of using this common construction material as a proxy for paleoenvironmental and archaeological studies. Both the molecular distribution of *n*-alkanes and bulk stable isotope compositions indicate that the ancient reeds were harvested from local sources and from habitats that were more diverse than those in northwestern China today. Moreover, due to a combination of early agriculture and natural climate forcing, the eastern edge of the Tarim Basin has experienced differential rates of environmental changes since the Han Dynasty, as the western side of Lop Nur became warmer and dryer at a faster pace. Our study demonstrates that given the excellent molecular preservation and common occurrence of *Phragmites* in archaeological sites, the reeds from the ancient Han era Great Walls in northwestern China hold outstanding potential to unlock environmental and climatic conditions on the western frontier during important periods in Chinese history.

## Methods

### Site Locations and Sampling

Ancient *Phragmites* culms and modern culms and leaves belonging to *P. australis* (Cavanilles) Trinius ex Steudel were collected from 14 sites in Gansu and Xinjiang (Fig. 1, Supplementary Table 1) during field expeditions in 2011 and 2016. Geographically, these sites are grouped as eastern (Sites 1-7) and western (Sites 8-14) clusters, separated by the now dried Lop Nur lake basin (Fig. 1B). Climatically, this region represents one of the driest areas in China with mean annual precipitation of only 66.5 mm at Yumen (40°16' N, 97°2' E) and 37.2 mm at Yuli (41°21' N, 86°16' E), localities representing the climate of the eastern and western side of the Lop Nur basin, respectively. There is also a regional mean annual temperature (MAT) difference, with MAT at Yumen being 7.5 °C compared to 12.1 °C of Yuli (see Supplementary Fig. 1). However, different paleoenvironmental proxies suggest wetter climate conditions with higher lake levels and precipitation in northwestern China during the Han Dynasty<sup>25-27,31,35,36,78-82</sup>. In contrast, lake records demonstrate decreased moisture availability and significant landscape change toward the end of the Han Dynasty and shortly afterwards<sup>31,33,82,83</sup>.

Ancient culms were sampled from exposed fascines of remnant wall segments, beacon towers, and fortification ruins (Fig. 2). The age of each location was determined using archaeological artifacts and historical documentation<sup>10-13</sup>. Wooden slips recovered from beacon towers at Yumenguan (Site 5, Fig. 1), Majuanwan (Site 7, Figs. 1 and 2A,B), and Dunhuang<sup>10,12</sup> date them to 111 – 108 BC. Precise ages for

the isolated beacon towers and fortifications of Xinjiang Province are uncommon, however. Yet, historical literature and archaeological remains attribute some of the western cluster sites to the Han Dynasty as well. For example, the “Book of the Later Han”<sup>14</sup> describes the construction of beacon towers along the Kongque River during the Emperor Wu period of the Han Dynasty (140 – 88 BC), which aligns with the archaeological record from the Lop Nur area<sup>10,11</sup>. It should be noted however, that a recent discovery of artifacts dating to the later Tang Dynasty (618 – 907 AD) from some beacon towers along the Kongque River suggests that they were subsequently garrisoned after the Han period (LY, unpublished data).

Most of the reed material used in construction are culms, as leaves have rarely been recovered from these ancient ruins (Fig. 2B). Modern, native *P. australis* was also sampled at six of the sites that contained reed stands near the ancient ruins to serve as modern correlates (Sites 1, 5, 7, 9, 10, 14; Fig. 1). Morphologically, the culms of ancient reeds are indistinguishable from their modern counterparts. All samples were kept frozen in the laboratory until analyzed.

## Plant Biomolecular Composition

### Molecular Composition

Modern ( $n=4$ ) and ancient ( $n=6$ ) plant samples were analyzed using Py-GC-MS to test for the molecular distributions and preservation of organic compounds at the Laboratory for Terrestrial Environments, Bryant University. Samples were pyrolyzed using a CDS 5250 Pyroprobe by combusting at 610 °C for 20 s to convert macromolecular compounds to GC amenable products. Compound detection and identification were performed using an Agilent 7890A GC System equipped with a Thermo TR-1 capillary column (60 m length, 0.25 mm i.d. and 0.25 µm film) coupled to a 5975C Series Mass Selective Detector (MSD). The GC oven was programmed from 40 °C (5 min hold) to 100 °C at 10 °C/min, then to 300 °C at 6 °C/min (25 min hold). Helium was the carrier gas with a constant flow of 1.1 mL/min. The MS source was operated at 250 °C with 70 eV ionization energy in the electron ionization (EI) mode and the MS Quadrupole mass analyzer was set to 150 °C with a scan rate of  $m/z$  50-500. Samples were held at the pyroprobe interface for at least 5 min at 300 °C for additional thermal extraction and to remove volatile impurities before gas chromatography. Compounds were identified by comparing their spectra with those reported in the literature<sup>84,85</sup>. Duplicate analyses of each sample was conducted for analytical consistency.

### Plant Wax Lipids

Plant culms and leaves were lyophilized and ground, then extracted with Dichloromethane:Methanol (9:1, v/v) using ultrasonication at 40 °C in three, 30-min cycles at the Institute of Earth Environment, Chinese Academy of Sciences. The total lipid extracts were dried under nitrogen and separated into two fractions through silica gel column chromatography using hexane and methanol, respectively, with  $n$ -alkanes being eluted in the hexane fraction. Quantification of  $n$ -alkanes was performed using an Agilent 6890 Series instrument equipped with a split-injector, HP1-ms GC column (60 m length, 0.32 mm i.d. and 0.25 µm film), and a Flame Ionization Detector (FID). Samples were injected in split mode (split ratio 4:1) and the GC oven was programmed from 40 °C (1 min hold) to 150 °C at 10 °C/min, then to 315 °C at 6 °C/min (20

min hold). Helium was the carrier gas with a constant flow of 1.2 mL/min. Peak areas were compared with an external standard mixture (C<sub>21</sub>-C<sub>33</sub>, odd numbered *n*-alkanes). Average chain length, or the weight-averaged number of carbon homologues of the C<sub>21</sub>-C<sub>33</sub> *n*-alkanes, was calculated as follows:

$$ACL = \frac{21(C_{21}) + 23(C_{23}) + \dots + 33(C_{33})}{C_{21} + C_{23} + \dots + C_{33}}$$

where C<sub>*x*</sub> is the abundance of the chain length with *x* carbons. The carbon preference index (CPI), which examines the odd-over-even carbon number predominance and serves as an indicator for hydrocarbon maturity and degradation<sup>86</sup>, was calculated using the abundances of odd and even chain lengths from C<sub>21</sub> to C<sub>33</sub> and the following formula:

$$CPI = \frac{(C_{21} + C_{23} + \dots + C_{31}) + (C_{23} + C_{25} + \dots + C_{33})}{2 \times (C_{22} + C_{24} + \dots + C_{32})}$$

Finally, two-tailed Student's t-Tests, assuming unequal variances, were used to test the significance in differences between sample sets (e.g., ancient vs. modern δ<sup>13</sup>C values).

## Bulk Carbon and Nitrogen Isotope Analysis

### Carbon

Culms from modern and ancient reeds were washed with distilled water and dried at 40°C before combustion (4h, 860°C) in a vacuum-sealed quartz tube in the presence of Ag foil and CuO. The purified CO<sub>2</sub> gas was then analyzed for carbon isotopes using a Finnigan MAT251 gas mass spectrometer. The national standard GBW04407 (δ<sup>13</sup>C<sub>VPDB</sub> = -22.43 ± 0.07‰) was analyzed between every twelve samples. The precision of repeated measurements of the laboratory standard was <0.1 ‰. Sample carbon isotope ratios (δ<sup>13</sup>C) are expressed as parts per thousand (‰) relative to the international VPDB standard and defined by the following equation:

$$\delta^{13}C = \left( \left( \frac{^{13}C}{^{12}C} \text{ Sample} \div \frac{^{13}C}{^{12}C} \text{ Standard} \right) - 1 \right) \times 1000$$

Since modern and ancient reed δ<sup>13</sup>C values were compared, +1.9 ‰ was added to all modern values<sup>87-89</sup> (Supplementary Table 1). This is to correct for the <sup>13</sup>C Suess effect, or the differences in atmospheric δ<sup>13</sup>C<sub>CO2</sub> between the value averaged for 2011 and 2016 of -8.4 ‰<sup>90</sup>, and the pre-industrial δ<sup>13</sup>C<sub>CO2</sub> value of -6.5‰<sup>91</sup>.

## Nitrogen

The nitrogen isotope ratios of the dried plant samples were determined at the Stable Isotope Biogeochemistry Laboratory at the Institute of Earth Environment, Chinese Academy of Sciences using a FLASH EA1112 elemental analyzer interfaced with a Delta-Plus continuous-flow isotope ratio mass spectrometer (IRMS). All of the  $\delta^{15}\text{N}$  values used a  $\text{KNO}_3$  reference material ( $\delta^{15}\text{N} +6.27 \text{‰}$ ) and an international isotope reference material (IAEA-N3;  $\delta^{15}\text{N} +4.70 \text{‰}$ ) to control the analytical accuracy of the EA-IRMS. Repeated analyses of the laboratory soil standards with confirmed  $\delta^{15}\text{N}$  values were performed daily to ensure instrumental accuracy. The standard deviation for repeated sample analyses was better than  $0.3 \text{‰}$ . The  $\delta^{15}\text{N}$  of each sample is expressed as ‰ relative to the international AIR standard and defined by the following equation:

$$\delta^{15}\text{N} = \left( \left( \frac{{}^{15}\text{N}}{{}^{14}\text{N}} \text{Sample} \div \frac{{}^{15}\text{N}}{{}^{14}\text{N}} \text{Standard} \right) - 1 \right) \times 1000$$

## Declarations

### Data availability

All data are available in the main text and the supplementary materials.

### Acknowledgements

We thank Xinyi Liu (Washington University in St. Louis) for reading an early version of the manuscript and providing constructive comments. Q.L. and H.Y. thank the support from Bryant University Summer Research Stipends and the Bryant Civilization Research Fund through the Charles J. Smiley Endowment. P.R. and R.P. would like to thank the Max Planck society for funding. M.S. thanks the European Research Council (ERC) under the European Union's Horizon 2020 research and innovation programme ('The Wall' project, grant agreement 882894). W.L. and H.W. thank the support from the Chinese Academy of Sciences (Grant No. XDB40000000), and this work was supported by the National Natural Science Foundation of China (Grant No. 41991252). Open access funding enabled and organized by Projekt DEAL.

### Author Contributions

R.P., Q.L., and H.Y. conceived the study; H.Y., Q.L., W.L., H.W., and L.Y. conducted field work and collected samples; R.P. and J. H. performed laboratory experiments; R.P., Q.L., H.Y., W.L., P.R., and M. S. analyzed data; all authors wrote and revised the manuscript.

### Competing Interests

The authors declare no competing interests.

## References

- 1 Needham, J., Ling, W. & Gwei-Djen, L. in *Science and Civilisation in China* (ed J. Needham) Ch. 28, 931 (Cambridge University Press, 1971).
- 2 Du, Y. *et al.* An exploration of the military defense system of the Ming Great Wall in Qinghai Province from the perspective of castle-based military settlements. *Archaeological and Anthropological Sciences* **13**, 1-18 (2021).
- 3 Liu, L. & Chen, X. *The Archaeology of China: From the Late Paleolithic to the Early Bronze Age*. (Cambridge University Press, 2012).
- 4 Lattimore, O. Origins of the Great Wall of China: A Frontier Concept in Theory and Practice. *Geographical Review* **27**, 539-549 (1937).
- 5 Di Cosmo, N. in *Ancient China and Its Enemies: The Rise of Nomadic Power in East Asian History* Ch. 4, 369 (Cambridge University Press, 2002).
- 6 Luo, L. *et al.* Identifying Linear Traces of the Han Dynasty Great Wall in Dunhuang Using Gaofen-1 Satellite Remote Sensing Imagery and the Hough Transform. *Remote Sensing* **11**, 1-22, doi:10.3390/rs11222711 (2019).
- 7 Waldron, A. *The Great Wall of China: From History to Myth*. (Cambridge University Press, 1990).
- 8 Xu, P. The Archaeology of the Great Wall of the Qin and Han Dynasties. *Journal of East Asian Archaeology* **3**, 259-281, doi:<https://doi.org/10.1163/156852301100402822> (2002).
- 9 Chen, T., Wang, X., Dai, J., Li, W. & Jiang, H. Plant use in the Lop Nor region of southern Xinjiang, China: Archaeobotanical studies of the Yingpan cemetery (~25–420 AD). *Quaternary International* **426**, 166-174, doi:<https://doi.org/10.1016/j.quaint.2016.03.015> (2016).
- 10 Lin, M. & Li, J. *Han Dynasty Slips along Shule River (in Chinese)*. (Wenwu Press, 1984).
- 11 Stein, M. A. Serindia Detailed Report of Explorations in Central Asia and Westernmost China. (1921).
- 12 Yue, B. & Zhong, S. *Survey report of Han Dynasty Great Walls along the Shule River (in Chinese)*. (Wenwu Press, 2001).
- 13 Wang, X.-y., Yao, Y. & Luo, L. A preliminary positioning of Yumen Pass of the Great Wall (Huanghuaying Section) in the Early Western Han Dynasty based on space archaeology: Responding to

- Stein's assumption of the location of Yumen Pass in beacon tower (No. T.XLII.d) 100 years ago. *Journal of Northwest University (Philosophy and Social Sciences Edition)* **51**, 16-26 (2021).
- 14 Fan, Y. in *Book of the Later Han* (ed Ye Fan) Ch. 87, (China Press, 1965).
- 15 Su, H. *et al.* The Great Wall of China: a physical barrier to gene flow? *Heredity* **90**, 212-219, doi:10.1038/sj.hdy.6800237 (2003).
- 16 Feng, L., Jia, Z. & Li, Q. The dynamic monitoring of aeolian desertification land distribution and its response to climate change in northern China. *Scientific Reports* **6**, 39563, doi:10.1038/srep39563 (2016).
- 17 Zhou, W. *et al.* Dynamic of grassland vegetation degradation and its quantitative assessment in the northwest China. *Acta Oecologica* **55**, 86-96, doi:<http://dx.doi.org/10.1016/j.actao.2013.12.006> (2014).
- 18 Chen, F. *et al.* Asian dust-storm activity dominated by Chinese dynasty changes since 2000 BP. *Nature Communications* **11**, 992, doi:10.1038/s41467-020-14765-4 (2020).
- 19 Yancheva, G. *et al.* Influence of the intertropical convergence zone on the East Asian monsoon. *Nature* **445**, 74-77, doi:10.1038/nature05431 (2007).
- 20 Luo, L. *et al.* Uncovering the ancient canal-based tuntian agricultural landscape at China's northwestern frontiers. *Journal of Cultural Heritage* **23**, 79-88, doi:<https://doi.org/10.1016/j.culher.2016.04.013> (2017).
- 21 Dai, S. *et al.* Vegetation cover change and the driving factors over northwest China. *Journal of Arid Land* **3**, 25-33, doi:10.3724/SP.J.1227.2011.00025 (2011).
- 22 Meng, H.-H., Gao, X.-Y., Huang, J.-F. & Zhang, M.-L. Plant phylogeography in arid Northwest China: Retrospectives and perspectives. *Journal of Systematics and Evolution* **53**, 33-46, doi:10.1111/jse.12088 (2015).
- 23 Mischke, S. *et al.* in *Socio-Environmental Dynamics along the Historical Silk Road* (eds L. E. Yang, X. Fang, H-R. Bork, & S. Mischke) Ch. 3, 45-66 (Springer Nature Switzerland, 2019).
- 24 Yang, X., Liu, Z., Zhang, F., White, P. D. & Wang, X. Hydrological changes and land degradation in the southern and eastern Tarim basin, Xinjiang, China. *Land Degradation & Development* **17**, 381-392, doi:<https://doi.org/10.1002/ldr.744> (2006).
- 25 Aichner, B., Feakins, S., Lee, J. E., Herzs Schuh, U. & Liu, X. High-resolution leaf wax carbon and hydrogen isotopic record of the late Holocene paleoclimate in arid Central Asia. *Climate of the Past* **11**, 619-633 (2015).

- 26 Lauterbach, S. *et al.* Climatic imprint of the mid-latitude Westerlies in the Central Tian Shan of Kyrgyzstan and teleconnections to North Atlantic climate variability during the last 6000 years. *The Holocene* **24**, 970-984, doi:10.1177/0959683614534741 (2014).
- 27 Liu, X., Herzschuh, U., Shen, J., Jiang, Q. & Xiao, X. Holocene environmental and climatic changes inferred from Wulungu Lake in northern Xinjiang, China. *Quaternary Research* **70**, 412-425, doi:10.1016/j.yqres.2008.06.005 (2008).
- 28 Mischke, S. & Wünnemann, B. The Holocene salinity history of Bosten Lake (Xinjiang, China) inferred from ostracod species assemblages and shell chemistry: Possible palaeoclimatic implications. *Quaternary International* **154-155**, 100-112, doi:<https://doi.org/10.1016/j.quaint.2006.02.014> (2006).
- 29 Mischke, S. *et al.* Modern hydrology and late Holocene history of Lake Karakul, eastern Pamirs (Tajikistan): A reconnaissance study. *Palaeogeography, Palaeoclimatology, Palaeoecology* **289**, 10-24, doi:<https://doi.org/10.1016/j.palaeo.2010.02.004> (2010).
- 30 Mischke, S., Lai, Z., Long, H. & Tian, F. Holocene climate and landscape change in the northeastern Tibetan Plateau foreland inferred from the Zhuyeze Lake record. *The Holocene* **26**, 643-654, doi:10.1177/0959683615612570 (2016).
- 31 Mischke, S. *et al.* The world's earliest Aral-Sea type disaster: the decline of the Loulan Kingdom in the Tarim Basin. *Scientific Reports* **7**, 43102, doi:10.1038/srep43102 (2017).
- 32 Ricketts, R. D., Johnson, T. C., Brown, E. T., Rasmussen, K. A. & Romanovsky, V. V. The Holocene paleolimnology of Lake Issyk-Kul, Kyrgyzstan: trace element and stable isotope composition of ostracodes. *Palaeogeography, Palaeoclimatology, Palaeoecology* **176**, 207-227, doi:[https://doi.org/10.1016/S0031-0182\(01\)00339-X](https://doi.org/10.1016/S0031-0182(01)00339-X) (2001).
- 33 Zhang, C., Feng, Z., Yang, Q., Gou, X. & Sun, F. Holocene environmental variations recorded by organic-related and carbonate-related proxies of the lacustrine sediments from Bosten Lake, northwestern China. *The Holocene* **20**, 363-373, doi:10.1177/0959683609353428 (2010).
- 34 Cheng, H. *et al.* The climatic cyclicity in semiarid-arid central Asia over the past 500,000 years. *Geophysical Research Letters* **39**, doi:<https://doi.org/10.1029/2011GL050202> (2012).
- 35 Wolff, C. *et al.* Precipitation evolution of Central Asia during the last 5000 years. *The Holocene* **27**, 142-154, doi:10.1177/0959683616652711 (2016).
- 36 Bao, Y., Braeuning, A., Yafeng, S. & Fahu, C. Evidence for a late Holocene warm and humid climate period and environmental characteristics in the arid zones of northwest China during 2.2 ~ 1.8 kyr B.P. *Journal of Geophysical Research: Atmospheres* **109**, doi:<https://doi.org/10.1029/2003JD003787> (2004).
- 37 Tandong, Y. & Thompson, L. G. Trends and features of climatic changes in the past 5000 years recorded by the Dunde ice core. *Annals of Glaciology* **16**, 21-24, doi:10.3189/1992AoG16-1-21-24 (1992).

- 38 Lü, H. *et al.* A preliminary study of chronology for a newly-discovered ancient city and five archaeological sites in Lop Nor, China. *Chinese Science Bulletin* **55**, 63-71, doi:10.1007/s11434-009-0586-4 (2010).
- 39 Qin, X. *et al.* New evidence of agricultural activity and environmental change associated with the ancient Loulan kingdom, China, around 1500 years ago. *The Holocene* **22**, 53-61, doi:10.1177/0959683611405234 (2011).
- 40 Lambertini, C. *et al.* A phylogeographic study of the cosmopolitan genus *Phragmites* (Poaceae) based on AFLPs. *Plant Systematics and Evolution* **258**, 161-182, doi:10.1007/s00606-006-0412-2 (2006).
- 41 Lessmann, J. M., Brix, H., Bauer, V., Clevering, O. A. & Comín, F. A. Effect of climatic gradients on the photosynthetic responses of four *Phragmites australis* populations. *Aquatic Botany* **69**, 109-126, doi:[https://doi.org/10.1016/S0304-3770\(01\)00133-4](https://doi.org/10.1016/S0304-3770(01)00133-4) (2001).
- 42 Zhang, T. & Wang, X. Stable Carbon Isotope and Long-Chain Alkane Compositions of the Major Plants and Sediment Organic Matter in the Yellow River Estuarine Wetlands. *Journal of Ocean University of China* **18**, 735-742, doi:10.1007/s11802-019-3918-2 (2019).
- 43 Liu, J., An, Z. & Liu, H. Leaf wax *n*-alkane distributions across plant types in the central Chinese Loess Plateau. *Organic Geochemistry* **125**, 260-269, doi:<https://doi.org/10.1016/j.orggeochem.2018.09.006> (2018).
- 44 Duan, Y. I. & He, J. Distribution and isotopic composition of *n*-alkanes from grass, reed and tree leaves along a latitudinal gradient in China. *Geochemical Journal* **45**, 199-207, doi:10.2343/geochemj.1.0115 (2011).
- 45 Li, J.-F. *et al.* Buried in Sands: Environmental Analysis at the Archaeological Site of Xiaohe Cemetery, Xinjiang, China. *PLOS ONE* **8**, e68957, doi:10.1371/journal.pone.0068957 (2013).
- 46 Zhang, J. *et al.* Phytoliths reveal the earliest fine reedy textile in China at the Tianluoshan site. *Scientific Reports* **6**, 18664, doi:10.1038/srep18664 (2016).
- 47 Zhang, G. *et al.* Ancient plant use and palaeoenvironmental analysis at the Gumugou Cemetery, Xinjiang, China: implication from desiccated plant remains. *Archaeological and Anthropological Sciences* **9**, 145-152, doi:10.1007/s12520-015-0246-3 (2015).
- 48 Ho, S., Wang, C., Wang, M. & Li, Z. Effect of petroleum on carbon and hydrogen isotopic composition of long-chain *n*-alkanes in plants from the Yellow River Delta, China. *Environmental Earth Sciences* **74**, 1603-1610, doi:10.1007/s12665-015-4161-9 (2015).
- 49 Bush, R. T. & McInerney, F. A. Leaf wax *n*-alkane distributions in and across modern plants: Implications for paleoecology and chemotaxonomy. *Geochimica et Cosmochimica Acta* **117**, 161-179 (2013).

- 50 Amundson, R. *et al.* Global patterns of the isotopic composition of soil and plant nitrogen. *Global Biogeochemical Cycles* **17**, doi:<https://doi.org/10.1029/2002GB001903> (2003).
- 51 Chen, Y., Takeuchi, K., Xu, C., Chen, Y. & Xu, Z. Regional climate change and its effects on river runoff in the Tarim Basin, China. *Hydrological Processes* **20**, 2207-2216, doi:<https://doi.org/10.1002/hyp.6200> (2006).
- 52 Tang, Q. C. & Chen, H. Y. Water resources and oasis construction in Tarim Basin. *Chinese Geographical Science* **2**, 173-182 (1992).
- 53 Zhou, W. J. *et al.* Environmental variability within the Chinese desert-loess transition zone over the last 20,000 years. *Holocene* **12**, 107-112, doi:[doi.org/10.1191/0959683602hl525rr](https://doi.org/10.1191/0959683602hl525rr) (2002).
- 54 Liu, W. & Wang, Z. Nitrogen isotopic composition of plant-soil in the Loess Plateau and its responding to environmental change. *Chinese Science Bulletin* **54**, 272-279 (2009).
- 55 Farquhar, G. D., Hubick, K. T., Condon, A. G. & Richards, R. A. in *Stable Isotopes in Ecological Research* Vol. 68 *Ecological Studies* (eds P. W. Rundel, J. R. Ehleringer, & K. A. Nagy) Ch. 21, 525 (Springer-Verlag, 1989).
- 56 Hou, J., D'Andrea, W. J., MacDonald, D. & Huang, Y. Evidence for water use efficiency as an important factor in determining the  $\delta D$  values of tree leaf waxes. *Organic Geochemistry* **38**, 1251-1255 (2007).
- 57 Cranwell, P. A. Lipid geochemistry of sediments from Upton Broad, a small productive lake. *Organic Geochemistry* **7**, 25-37 (1984).
- 58 Tipple, B. J. & Pagani, M. Environmental control on eastern broadleaf forest species' leaf wax distributions and D/H ratios. *Geochimica et Cosmochimica Acta* **111**, 64-77 (2013).
- 59 Bush, R. T. & McInerney, F. A. Influence of temperature and  $C_4$  abundance on *n*-alkane chain length distributions across the central USA. *Organic Geochemistry* **79**, 65-73 (2015).
- 60 Castañeda, I. S., Werne, J. P., Johnson, T. C. & Filley, T. R. Late Quaternary vegetation history of southeast Africa: The molecular isotopic record from Lake Malawi. *Palaeogeography, Palaeoclimatology, Palaeoecology* **275**, 100-112, doi:<https://doi.org/10.1016/j.palaeo.2009.02.008> (2009).
- 61 Dodd, R. S. & Poveda, M. M. Environmental gradients and population divergence contribute to variation in cuticular wax composition in *Juniperus communis*. *Biochemical Systematics and Ecology* **31**, 1257-1270, doi:[https://doi.org/10.1016/S0305-1978\(03\)00031-0](https://doi.org/10.1016/S0305-1978(03)00031-0) (2003).
- 62 Carr, A. S. *et al.* Leaf wax *n*-alkane distributions in arid zone South African flora: Environmental controls, chemotaxonomy and palaeoecological implications. *Organic Geochemistry* **67**, 72-84, doi:<https://doi.org/10.1016/j.orggeochem.2013.12.004> (2014).

- 63 Sachse, D., Radke, J. & Gleixner, G.  $\delta$ D values of individual *n*-alkanes from terrestrial plants along a climatic gradient – Implications for the sedimentary biomarker record. *Organic Geochemistry* **37**, 469-483 (2006).
- 64 Barnes, M. A. & Barnes, W. C. in *Lakes: Chemistry, Geology, Physics* (ed A. Lerman) 127-152 (Springer-Verlag, 1978).
- 65 Ficken, K. J., Li, B., Swain, D. L. & Eglinton, G. An *n*-alkane proxy for the sedimentary input of submerged/floating freshwater aquatic macrophytes. *Organic Geochemistry* **31**, 745-749 (2000).
- 66 Chikaraishi, Y. & Naraoka, H.  $\delta^{13}\text{C}$  and  $\delta\text{D}$  relationships among three *n*-alkyl compound classes (*n*-alkanoic acid, *n*-alkane and *n*-alkanol) of terrestrial higher plants. *Organic Geochemistry* **38**, 198-215 (2007).
- 67 Eglinton, G. & Hamilton, R. J. Leaf epicuticular waxes. *Science* **156**, 1322-1335 (1967).
- 68 Aichner, B., Herzsuh, U. & Wilkes, H. Influence of aquatic macrophytes on stable carbon isotope signatures of sedimentary organic matter in lakes on the Tibetan Plateau. *Organic Geochemistry* **41**, 706-718 (2010).
- 69 Bingham, E. M. *et al.* Conservative composition of *n*-alkane biomarkers in Sphagnum species: Implications for palaeoclimate reconstruction in ombrotrophic peat bogs. *Organic Geochemistry* **41**, 214-220, doi:<https://doi.org/10.1016/j.orggeochem.2009.06.010> (2010).
- 70 Huang, Y., Shuman, B., Wang, Y. & Webb III, T. Hydrogen isotope ratios of palmitic acid in lacustrine sediments record late Quaternary climate variations. *Geology* **30**, 1103-1106 (2002).
- 71 Shepherd, T. & Wynne Griffiths, D. The effects of stress on plant cuticular waxes. *New Phytologist* **171**, 469-499, doi:<https://doi.org/10.1111/j.1469-8137.2006.01826.x> (2006).
- 72 Nowakowski, D. J., Woodbridge, C. R. & Jones, J. M. Phosphorus catalysis in the pyrolysis behaviour of biomass. *Journal of Analytical and Applied Pyrolysis* **83**, 197-204, doi:<https://doi.org/10.1016/j.jaap.2008.08.003> (2008).
- 73 Jia, L. *et al.* Fast Pyrolysis of Heartwood, Sapwood, and Bark: A Complementary Application of Online Photoionization Mass Spectrometry and Conventional Pyrolysis Gas Chromatography/Mass Spectrometry. *Energy & Fuels* **31**, 4078-4089, doi:10.1021/acs.energyfuels.7b00110 (2017).
- 74 Johannisson, C. & Högberg, P.  $^{15}\text{N}$  abundance of soils and plants along an experimentally induced forest nitrogen supply gradient. *Oecologia* **97**, 322-325, doi:10.1007/BF00317321 (1994).
- 75 Choi, W.-J., Chang, S. X., Allen, H. L., Kelting, D. L. & Ro, H.-M. Irrigation and fertilization effects on foliar and soil carbon and nitrogen isotope ratios in a loblolly pine stand. *Forest Ecology and Management* **213**, 90-101, doi:<https://doi.org/10.1016/j.foreco.2005.03.016> (2005).

- 76 Marshall, F. *et al.* Ancient herders enriched and restructured African grasslands. *Nature* **561**, 387-390, doi:[10.1038/s41586-018-0456-9](https://doi.org/10.1038/s41586-018-0456-9) (2018).
- 77 Szpak, P., Millaire, J.-F., White, C. D. & Longstaffe, F. J. Influence of seabird guano and camelid dung fertilization on the nitrogen isotopic composition of field-grown maize (*Zea mays*). *Journal of Archaeological Science* **39**, 3721-3740, doi:<https://doi.org/10.1016/j.jas.2012.06.035> (2012).
- 78 Wang, W., Feng, Z., Ran, M. & Zhang, C. Holocene climate and vegetation changes inferred from pollen records of Lake Aibi, northern Xinjiang, China: A potential contribution to understanding of Holocene climate pattern in East-central Asia. *Quaternary International* **311**, 54-62, doi:<https://doi.org/10.1016/j.quaint.2013.07.034> (2013).
- 79 Rhodes, T. E. *et al.* A Late Pleistocene-Holocene lacustrine record from Lake Manas, Zunggar (northern Xinjiang, western China). *Palaeogeography, Palaeoclimatology, Palaeoecology* **120**, 105-121, doi:[https://doi.org/10.1016/0031-0182\(95\)00037-2](https://doi.org/10.1016/0031-0182(95)00037-2) (1996).
- 80 Fan, Q., Ma, H., Wei, H. & An, F. Holocene lake-level changes of Hurlig Lake on northeastern Qinghai-Tibetan Plateau and possible forcing mechanism. *The Holocene* **24**, 274-283, doi:[10.1177/0959683613517399](https://doi.org/10.1177/0959683613517399) (2014).
- 81 Liu, X.-J., Lai, Z., Madsen, D. & Zeng, F. Last deglacial and Holocene lake level variations of Qinghai Lake, north-eastern Qinghai-Tibetan Plateau. *Journal of Quaternary Science* **30**, 245-257, doi:<https://doi.org/10.1002/jqs.2777> (2015).
- 82 Herzsuh, U., Tarasov, P., Wünnemann, B. & Hartmann, K. Holocene vegetation and climate of the Alashan Plateau, NW China, reconstructed from pollen data. *Palaeogeography, Palaeoclimatology, Palaeoecology* **211**, 1-17, doi:<https://doi.org/10.1016/j.palaeo.2004.04.001> (2004).
- 83 Long, H., Lai, Z., Fuchs, M., Zhang, J. & Li, Y. Timing of Late Quaternary palaeolake evolution in Tengger Desert of northern China and its possible forcing mechanisms. *Global and Planetary Change* **92-93**, 119-129, doi:<https://doi.org/10.1016/j.gloplacha.2012.05.014> (2012).
- 84 Gupta, N. S. *et al.* Diagenesis of plant biopolymers: Decay and macromolecular preservation of *Metasequoia*. *Organic Geochemistry* **40**, 802-809 (2009).
- 85 Ralph, J. & Hatfield, R. D. Pyrolysis-GC-MS characterization of forage materials. *Journal of Agriculture Food Chemistry* **39**, 1426-1437 (1991).
- 86 Duan, Y. & Xu, L. Distributions of *n*-alkanes and their hydrogen isotopic composition in plants from Lake Qinghai (China) and the surrounding area. *Applied Geochemistry* **27**, 806-814 (2012).
- 87 Verburg, P. The need to correct for the Suess effect in the application of  $\delta^{13}\text{C}$  in sediment of autotrophic Lake Tanganyika, as a productivity proxy in the Anthropocene. *Journal of Paleolimnology* **37**,

591-602, doi:10.1007/s10933-006-9056-z (2007).

88 Hare, V. J., Loftus, E., Jeffrey, A. & Ramsey, C. B. Atmospheric CO<sub>2</sub> effect on stable carbon isotope composition of terrestrial fossil archives. *Nature communications* **9**, 252-252, doi:10.1038/s41467-017-02691-x (2018).

89 Francey, R. J. *et al.* A 1000-year high precision record of  $\delta^{13}\text{C}$  in atmospheric CO<sub>2</sub>. *Tellus B: Chemical and Physical Meteorology* **51**, 170-193, doi:10.3402/tellusb.v51i2.16269 (1999).

90 Keeling, C. D. *et al.* Exchanges of atmospheric CO<sub>2</sub> and <sup>13</sup>CO<sub>2</sub> with the terrestrial biosphere and oceans from 1978 to 2000. 88 (Scripps Institution of Oceanography, San Diego, 2001).

91 Tipple, B. J., Meyers, S. R. & Pagani, M. Carbon isotope ratio of Cenozoic CO<sub>2</sub>: A comparative evaluation of available geochemical proxies. *Paleoceanography* **25**, 1-11 (2010).

## Figures

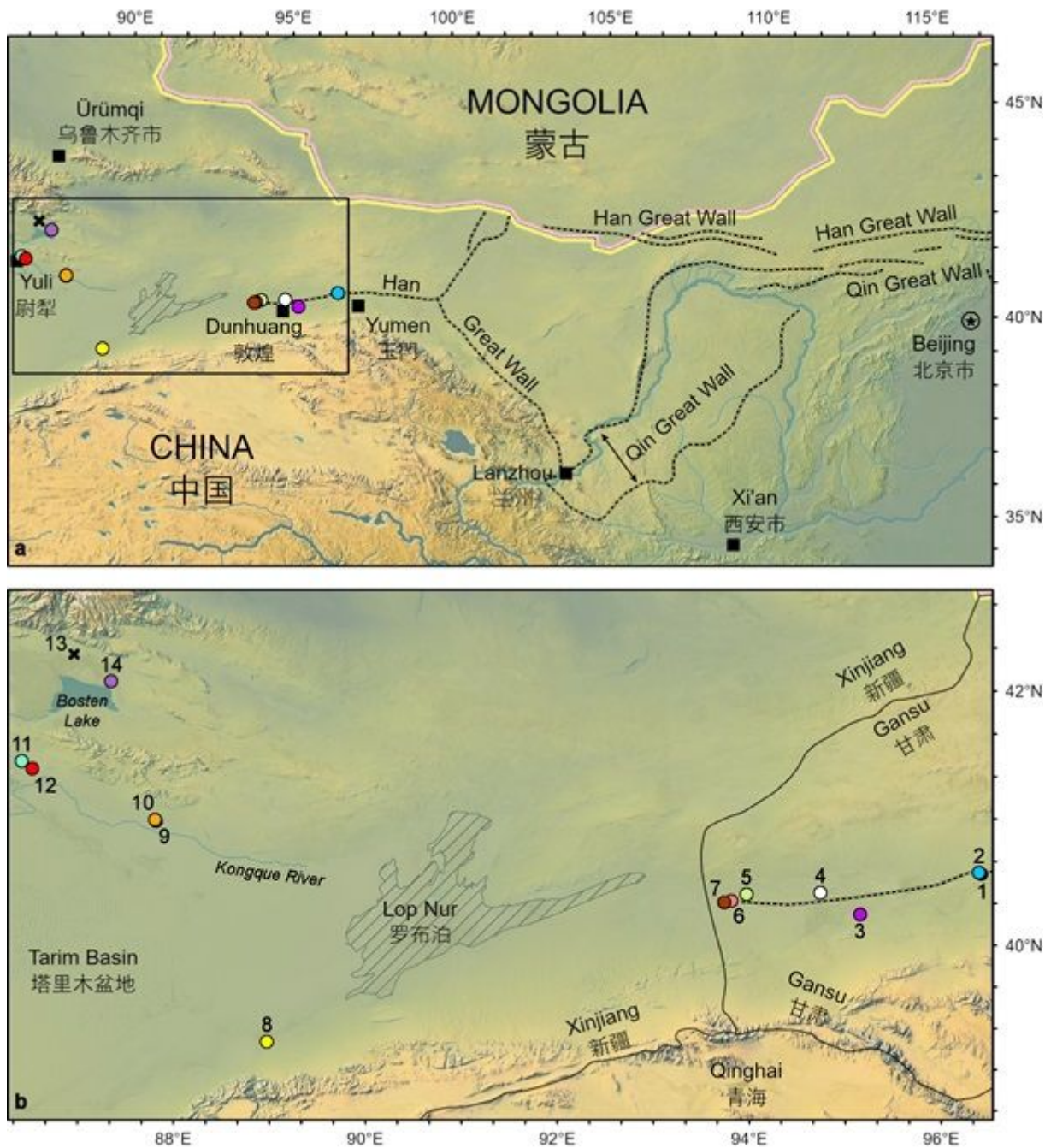


**Figure 1**

Map showing the extent of the Great Wall dated to the Qin and Han dynasties. a. Extent of the Great Wall dated to the Qin and Han dynasties in northern China. b. Sampling locations in Gansu and Xinjiang provinces: (1) Han Dynasty Great Wall segment; (2), Beacon tower near Site 1; (3) Beacon tower near Guazhou town; (4) Xijiandun Beacon Tower; (5) Cang Ting Sui Beacon Tower at Yumenguan; (6) Great Wall Heritage Site; (7); (8) Milan Castle Heritage Site; (9) Buddha Tower, south end of the Yingpan City Heritage Site; (10) City wall, north end of the Yingpan City Heritage Site; (11) Yakelun Beacon Tower; (12) Sunji Beacon Tower; (13) Tahaqi Beacon Tower; (14) Sishilidadun Beacon Tower. Note: The designations employed and the presentation of the material on this map do not imply the expression of any opinion whatsoever on the part of Research Square concerning the legal status of any country, territory, city or

area or of its authorities, or concerning the delimitation of its frontiers or boundaries. This map has been provided by the authors.



**Figure 2**

Remnant wall segments and beacon towers of northwestern China. a. Wall section at Majuanwan (Site 7); b. Grass fascines alternating with layers of rammed earth at Majuanwan; c. Sishilidadun Beacon Tower (Site 14); d. Low altitude air photo of the Yakelun Beacon Tower (Site 11), courtesy of Xingjun Hu.

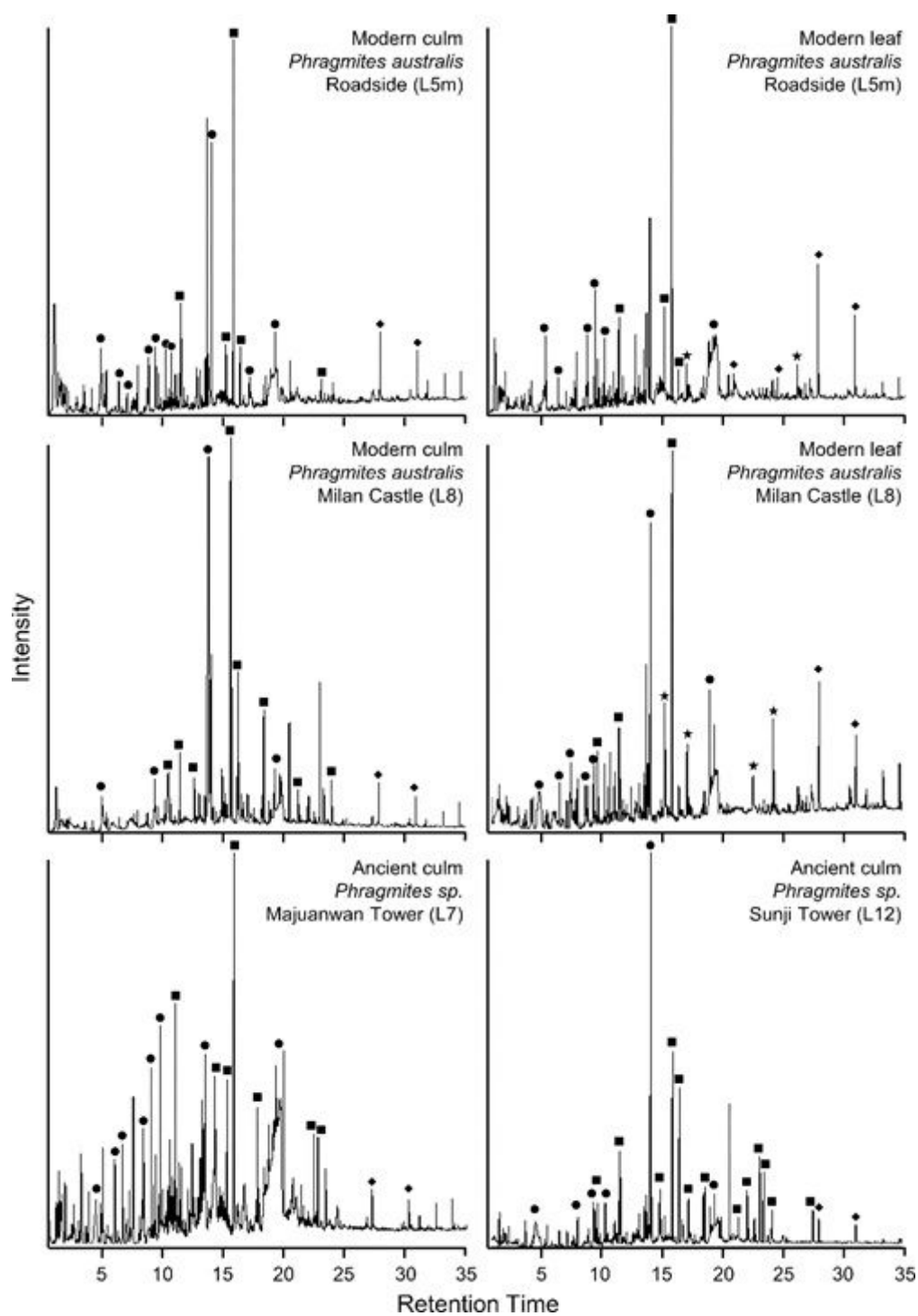


**Figure 3**

Partial ion chromatograms. The Py-GC-MS analysis of modern and ancient *Phragmites* culms and leaves and the distribution of ● Polysaccharide, ■ Lignin, ◆ Fatty Acid, and □ Amino Acid. See Supplementary Table 2 for compound identifications.

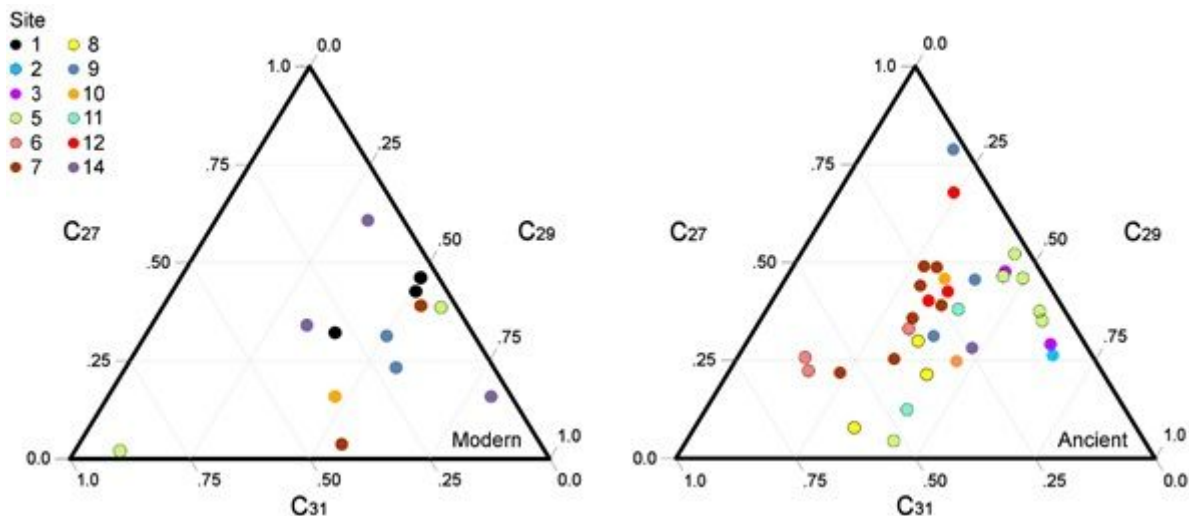


**Figure 4**

Ternary diagrams of the C27, C29, and C31 n-alkane abundances for modern and ancient reeds. Site number corresponds to locations and colour scheme of Figure 1.

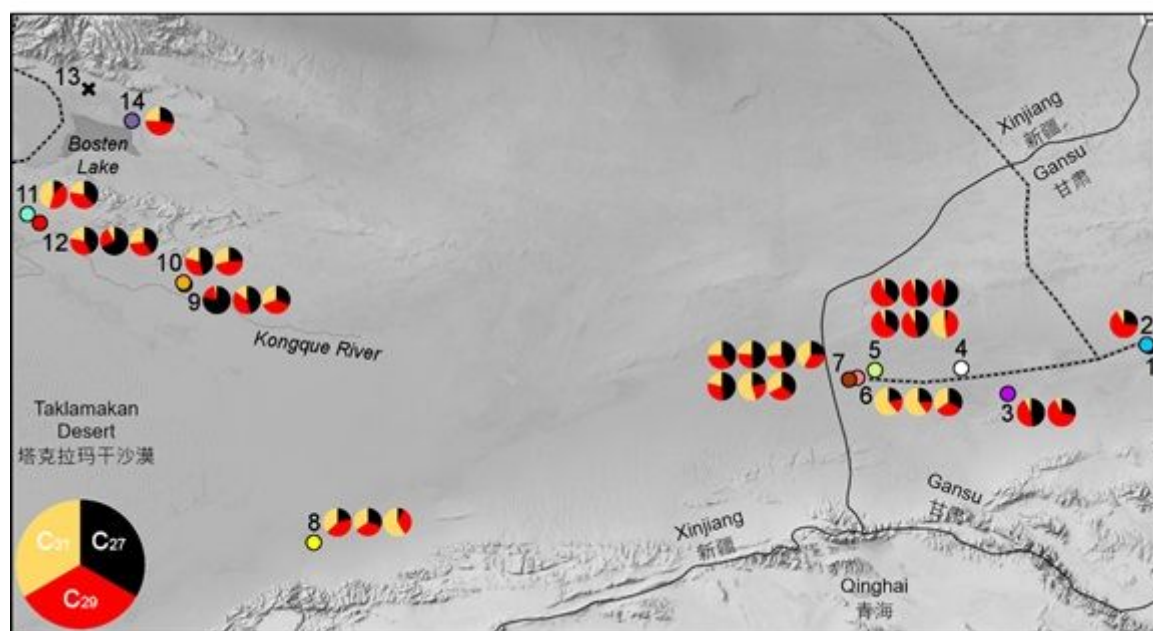


**Figure 5**

Site-specific C27, C29, and C31 n-alkane abundances. Pie chart represents the relative percentage of the three most dominant n-alkanes in each ancient reed sample from Great Wall segments and beacon towers. The higher variation in n-alkane distribution suggests greater ecological diversity in during wall building phases. Note: The designations employed and the presentation of the material on this map do not imply the expression of any opinion whatsoever on the part of Research Square concerning the legal status of any country, territory, city or area or of its authorities, or concerning the delimitation of its frontiers or boundaries. This map has been provided by the authors.

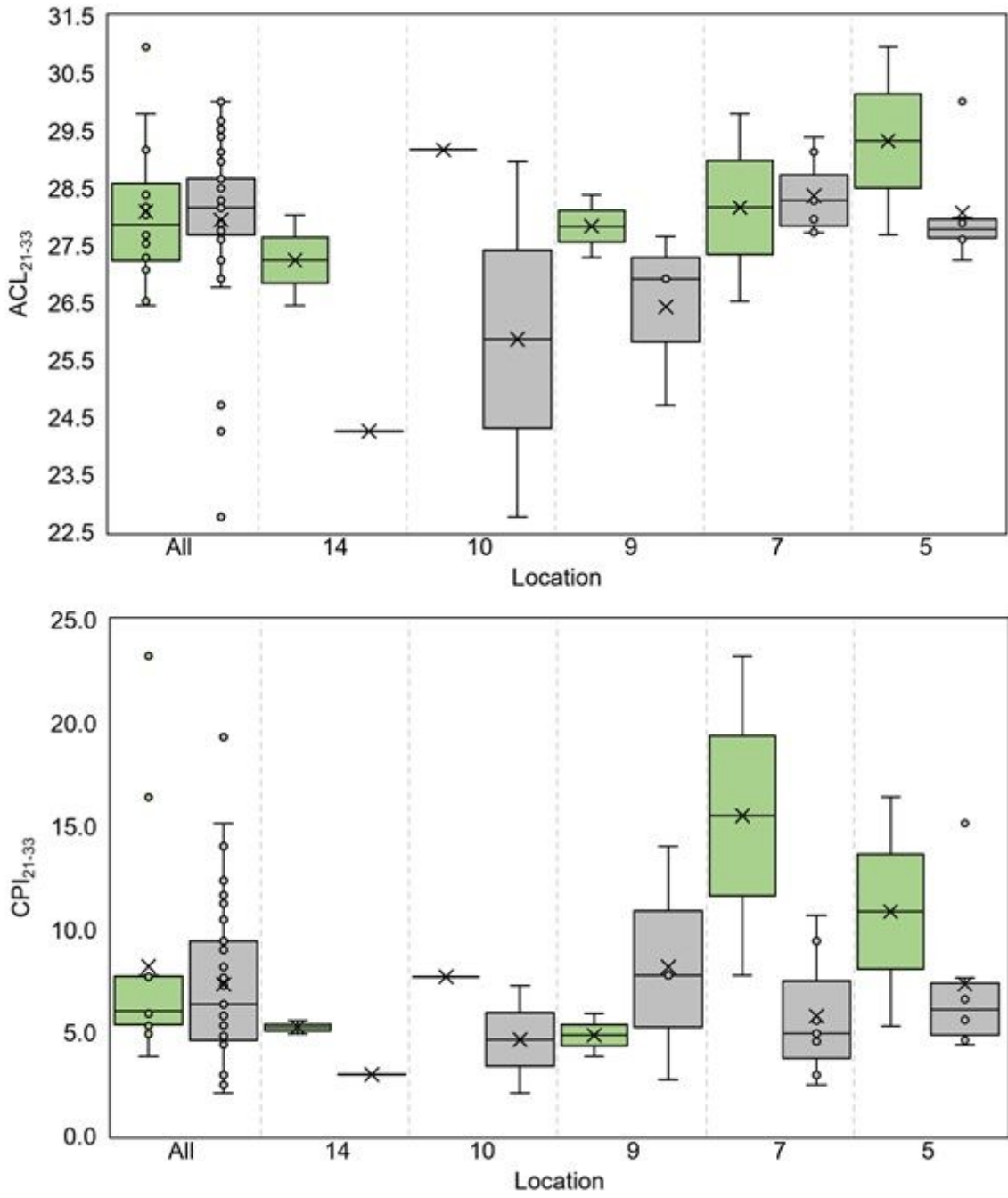


**Figure 6**

Box plots by location for modern (green) and ancient (gray) reeds. Top: average chain length (ACL). Bottom: carbon preference index (CPI). Location number corresponds to sites from Figure 1.

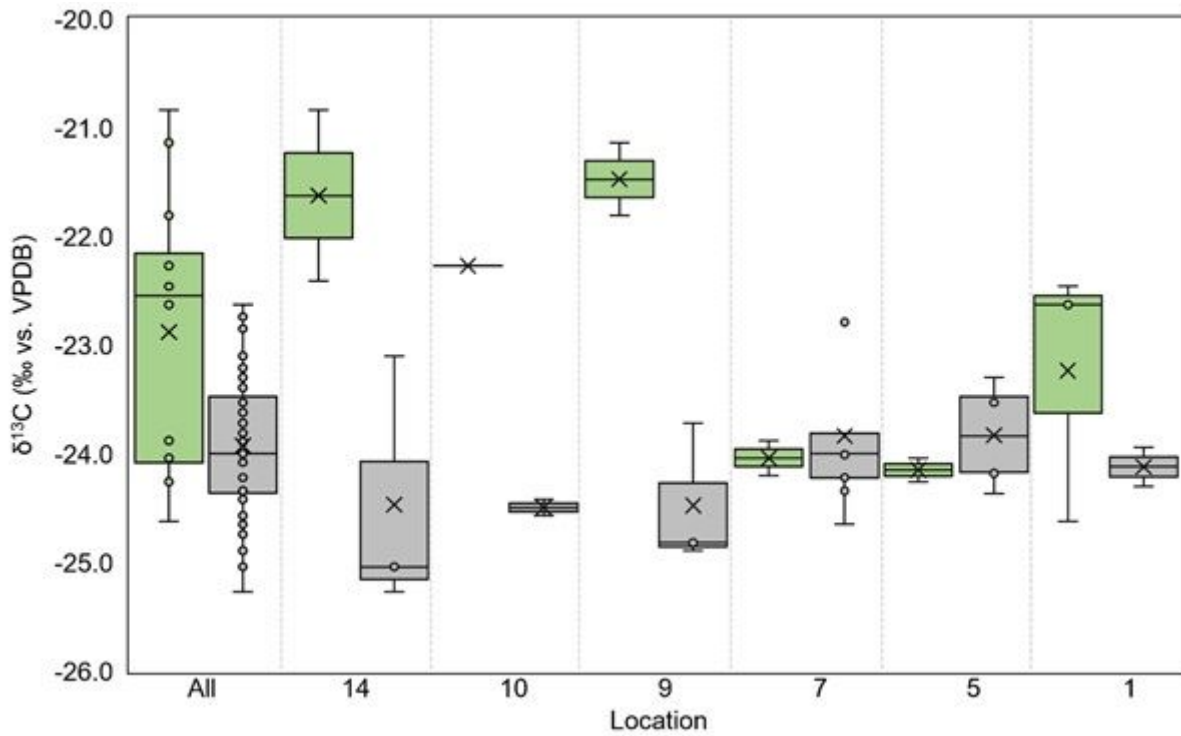


**Figure 7**

Box plot by location for bulk  $\delta^{13}\text{C}$  for modern (green) and ancient (gray) reeds. Only sites where both modern and ancient grasses were collected. Location number corresponds to sites from Figure 1.

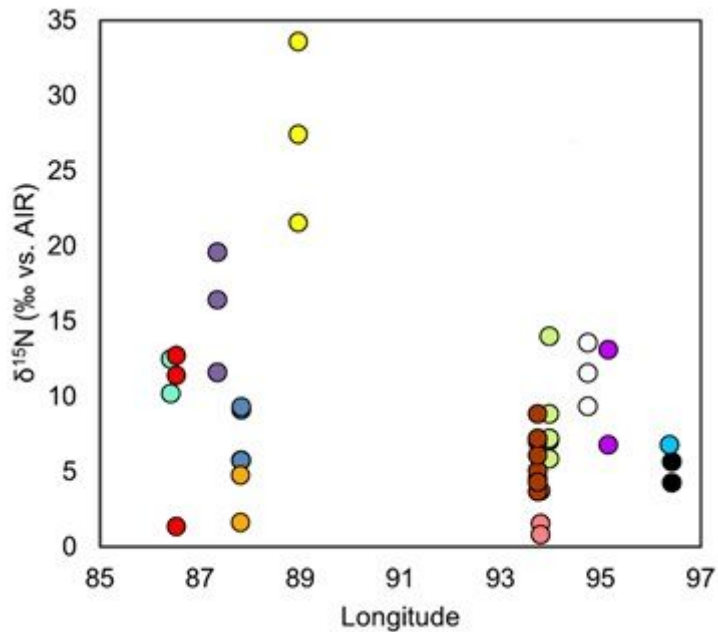


**Figure 8**

Bulk  $\delta^{15}\text{N}$  of ancient grasses by longitude. Color of the circles corresponds to site location from Figure 1. Western cluster sites between 85° and 90°, eastern cluster sites between 93° and 97°.

## Supplementary Files

This is a list of supplementary files associated with this preprint. Click to download.

- [SIFigure1.tif](#)
- [SIFigure2.tif](#)
- [SIFigure3.tif](#)
- [SupplementaryTable1.xlsx](#)
- [SupplementaryTable2.xlsx](#)